J Eng Math (2010) 66:271–292
DOI 10.1007/s10665-009-9313-z

Coarsening dynamics of slipping droplets

Georgy Kitavtsev · Barbara Wagner

Received: 30 September 2008 / Accepted: 29 June 2009 / Published online: 18 July 2009

Abstract The late-phase dewetting process of nanoscopic thin polymer films on hydrophobized substrates using some recently derived lubrication models that take account of large slippage at the polymer-substrate interface is studied. The late phase of this process is characterized by the slow-time coarsening dynamics of arrays of droplets that remain after rupture and the initial dewetting phases. For this situation a reduced system of ordinary differential equations is derived from the lubrication model for large slippage using asymptotic analysis. This extends known results for the no-slip case. On the basis of the reduced model, the role of the slippage as a control parameter for droplet migration is analysed and several new qualitative effects for the coarsening process are identified.

Keywords Coarsening · Fluid dynamics · Lubrication models · Wall slippage

1 Introduction

A liquid polymer film of nanometer thickness interacting with a hydrophobically coated solid substrate is susceptible to instability due to small perturbations of the film profile. Typically such films rupture, thereby initiating a complex dewetting process [1–5]. The influence of intermolecular forces plays an important part in the rupture and subsequent dewetting process; see e.g. [6–8] and references therein. Due to the small thickness of the film, the competition between the long-range attractive van der Waals and short-range Born repulsive intermolecular forces reduces the unstable film to an even thinner layer of thickness ε that connects the evolving patterns and is closely related to the minimum of the corresponding intermolecular potential, i.e., the film settles into an energetically more favorable state [9,10]. The early stages of this process are associated with the formation of regions of this minimal thickness, bounded by moving rims that connect to the undisturbed film and eventually destabilize [11–13].

In this study we are interested in the long-time dewetting process, which originates in the breaking up of the evolving patterns into small droplets and is characterized by its subsequent slow-time coarsening dynamics, which has been observed and investigated experimentally in [14,15]. Within a different context of phase separation of binary

G. Kitavtsev
Institute of Mathematics, Humboldt University of Berlin, 10099 Berlin, Germany
e-mail: kitavtsg@math.hu-berlin.de

B. Wagner (✉)
Weierstrass Institute for Applied Analysis and Stochastics, Mohrenstraße 39, 10117 Berlin, Germany
e-mail: wagnerb@wias-berlin.de

alloys, coarsening dynamics is a well-known widely studied process and is typically described by the Cahn–Hilliard equation [16]. For the late phases of this process the existence of metastable solutions were first shown in [17], and after that reduced ODE models have been derived and investigated in [18–20] that allow to determine properties such as coarsening rates, which can be time-consuming using the underlying partial differential equations. These studies have recently been extended to describe phase separation under the influence of an external driving field in [21,22]. Within the context of thin liquid films one of the first studies of the coarsening dynamics can be found in [23] and [24]. These authors consider the one-dimensional no-slip lubrication model for the profile $h(x,t)$,

$$\partial_t h = -\partial_x \left(h^3 \partial_x \left(\partial_{xx} h - \Pi(h) \right) \right) \tag{1.1}$$

and, using asymptotic methods, derive a reduced model that is able to describe the slow-time coarsening process for large arrays of droplets, including mechanisms such as collapse as well as collisions of droplets, and predict their coarsening rate.

Let us recall that the high order of the lubrication equation (1.1) is a result of the contribution from surface tension at the free boundary, reflected by the linearized curvature term $\partial_{xx} h$. A further contribution to the pressure arises from the intermolecular forces and is denoted by $\Pi(h)$. A commonly used expression is given by

$$\Pi(h) = \frac{1}{\varepsilon} \left[\left(\frac{\epsilon}{h} \right)^n - \left(\frac{\varepsilon}{h} \right)^{m+n-1} \right], \tag{1.2}$$

with $n = 3$ and $m = 2$ being typical values. It can be written as a derivative of the potential function $U(h)$,

$$U(h) = \frac{1}{3} \left(\frac{\varepsilon}{h} \right)^{m+n-2} - \frac{1}{2} \left(\frac{\varepsilon}{h} \right)^{n-1}, \tag{1.3}$$

where the minimal thickness between the droplets is of order $0 < \varepsilon \ll 1$.

Recently, it has been shown experimentally and theoretically that the early stages of the dewetting process and the evolving morphology depend markedly on the magnitude of the effective slip length, which can be of the size of the height of the liquid film or even larger for nanoscale systems [13,25–28]. In order to understand this behavior, closed-form lubrication models over a wide range of slip lengths were derived in [29,30] from the underlying equations for conservation of mass and momentum, together with boundary conditions for the tangential and normal stress, as well as the kinematic condition at the free boundary, impermeability and Navier-slip condition at the liquid–solid interface.

In the context of the physical application of polymer melts dewetting from a substrate that is hydrophobically coated with polymer brushes, we assume that the complex microscopic dynamics involved here, can be described by an effective Navier-slip condition

$$u^* = b^* \, \partial_{z^*} u^* \quad \text{at } z^* = 0 \tag{1.4}$$

on the macroscopic, continuum level, given here in dimensional form. It states that the lateral velocity u^* is proportional to the shear rate $\partial_{z^*} u^*$, with proportionality constant b^*, the effective slip-length parameter, having the dimension of a length. In the rest of the paper it nondimensionalized by the typical height h^* of the undisturbed film $b^* = h^* b$.

Asymptotic arguments, based on the magnitude of the slip length show that within a lubrication scaling there are two *distinguished limits* [29]:

These are the well-known *weak-slip* model

$$\partial_t h = -\partial_x \left(M(h) \partial_x \left(\partial_{xx} h - \Pi(h) \right) \right), \tag{1.5}$$

where $M(h) = h^3 + bh^2$ with b denoting the slip-length parameter, and the *strong-slip* model

$$\mathrm{Re} \left(\partial_t u + u \partial_x u \right) = \frac{4}{h} \partial_x (h \partial_x u) + \partial_x \left(\partial_{xx} h - \Pi(h) \right) - \frac{u}{\beta h}, \tag{1.6a}$$

$$\partial_t h = -\partial_x (hu), \tag{1.6b}$$

respectively. Here, $u(x,t)$ denotes the velocity in the lateral direction. The slip-length parameters b and β are related by orders of magnitude via $b \sim \nu^2 \beta$, where the parameter ν with $0 < \nu \ll 1$ refers to the vertical to horizontal scale

separation of the thin film. The terms Re $(\partial_t u + u\partial_x u)$, with Re denoting the Reynolds number, and $(4/h)\partial_x(h\,\partial_x u)$ are the inertial and Trouton viscosity terms, respectively.

Additionally, the weak-slip and the strong-slip models contain as limiting cases three further lubrication models. One is the no-slip model which is obtained when we set $b = 0$ in the weak-slip model. The second one is obtained from the strong-slip model in the limit $\beta \to \infty$ and describes the dynamics of suspended free films; see e.g. [31]. For the third limiting case derived in [29] the slip-length parameter β_I is of an order of magnitude lying in between those that lead to the weak and the strong-slip model, i.e., $b \ll \beta_I \ll \beta$. The corresponding *intermediate-slip* model is given by

$$\partial_t h = -\partial_x \left(h^2 \partial_x \left(\partial_{xx} h - \Pi(h) \right) \right). \tag{1.7}$$

It can be obtained by rescaling time in (1.5) by b and letting $b \to \infty$ or by rescaling time and the horizontal velocity by β and taking the limit $\beta \to 0$.

In view of the above developments, we would like to understand the effects of slippage during the late stages of the dewetting process, such as the details of coarsening mechanisms. Moreover, we would like to know if it is possible to obtain reduced models to answer these questions. Hence, in this paper we will focus our investigations on the lubrication models for the slip-regimes, (1.7) and (1.6a)–(1.6b). It turns out that in the case of the intermediate-slip model (1.7) the derivation of a corresponding reduced ODE model for the position and pressure of arrays of droplets can be obtained by following the ideas in [23], so that we only briefly summarize our results and focus here mainly on the strong-slip model.

Additionally, using essentially a mixture of the gradient flow structure approach and asymptotic analysis, the one- as well as the two-dimensional case for $M(h) = h^q$, $q > 0$ has recently been considered in [32]. Within the context of thin liquid films the relevant case here is $M(h) = h^2$, the intermediate-slip model, apart form the more frequently considered no-slip case when $M(h) = h^3$. We note that, within the different context of Darcy's equation, also the case $M(h) = h$ was considered in [33], where coarsening rates on the basis of the gradient flow structure of the corresponding equation were derived. Moreover, for this case they showed that the analysis can be made rigorous. One focus of the recent work [32] concerned migration of the droplets and its underlying causes, where results reported in [34] on the relation between directions of the motion and of the mass flux were discussed and clarified, i.e., that indeed the direction of the migration of droplets is opposite to the applied mass flux. We also like to note at this point that, in light of the derivation of the lubrication models for various slip regimes as given in [29], the no- and intermediate-slip lubrication equations arise from different balances of the underlying governing equations. As a consequence, when comparing results for the two models, as done in [32, Appendix D], the actual physical interpretation of properties such as migration velocities needs to take into account the different time scales of these regimes.

Finally, in a recent paper [35] the results of [23] were extended to the two-dimensional case and a comparison with an alternative derivation from [32] were given. A very interesting extension that includes gravity, which becomes important as some droplets get larger, is given and analysed in [36].

In this article, we begin with the derivation of the steady states for the strong-slip model and its limiting cases in Sect. 2. In Sect. 3.2 for the one-dimensional strong-slip model with sufficiently small inertial terms we then derive a reduced model. In Sect. 3.3 we derive an approximation for the fluxes between droplets in an array. In Sect. 4.3 (Proposition 4.1) we prove that, in contrast to the no- and intermediate-slip cases, which were treated in [32] for any mobility h^q, $q > 0$, in the strong-slip case droplets do not necessarily migrate in the direction opposite to the applied flux. There is a critical value of slippage $\beta = \beta_{\text{crit}}$ above which droplets migrate in the same direction as the flux. As a further consequence of that we find that collisions of two droplets are possible for some range of slip parameter β in the model (1.6a)–(1.6b), while for the models (1.1), (1.5) and (1.7) it was shown in [24,32] that collisions involve at least three droplets.

Section 4.4 is devoted to the resulting coarsening patterns for increasing slippage. Here, we identified another new effect in the strong-slip case. For the models (1.1) and (1.7) it was shown in [32] that the collision component of the coarsening process is comparable with the component for collapse only in the case of (1.1), while it is negligible for (1.7). For the strong-slip model this component increases when β increases and becomes the dominant component

of the coarsening process. In the Sect. 4.5 we make numerical simulations of coarsening rates for the strong-slip case using the corresponding reduced model and find that their slope changes with the slip-length $\beta > 0$.

2 Equilibrium and near-equilibrium solutions

2.1 Equilibrium solutions

Let us briefly revisit the initial-boundary-value problem for the weak-slip model (1.5) on an interval $[-L, L]$. We impose the following boundary conditions:

$$\partial_{xxx} h = 0, \quad \text{and} \quad \partial_x h = 0 \quad \text{at } x = \pm L, \tag{2.1}$$

which incorporate zero flux at the boundary and as a consequence imply conservation of mass law (2.2):

$$\tilde{h} = \frac{1}{2L} \int_{-L}^{+L} h(x,t)\,\mathrm{d}x, \quad \forall t > 0, \tag{2.2}$$

where $\tilde{h} = \text{const}$ is the average of the height profile. For these boundary conditions it has been proved in [10] that (1.5) has a unique strong positive solution, for the initial data $h(0,x) > 0$ and $h(0,x) \in H^1(-L, L)$. For our subsequent analysis it will be useful to summarize their results on equilibrium solutions ([10, 23]) here:

Theorem 2.1 *Equation* (1.5) *under boundary conditions* (2.1) *has a family of positive nonconstant steady state solutions* $\bar{h}(x, P, L)$ *parameterized by the constant pressure* P *and given by the solution of*

$$P = \Pi\left(\bar{h}\right) - \partial_{xx}\bar{h}, \tag{2.3a}$$

$$0 = \partial_x \bar{h}(-L) = \partial_x \bar{h}(L). \tag{2.3b}$$

Moreover, phase-plane analysis shows that for fixed value $P \in (0, P_{\max})$ the ODE (2.3a) has a family of periodic solutions $\bar{h}(x, P, L)$ parameterized by the least period $T = 2L$ that is nested into a homoclinic loop $\bar{h}(x, P)$. Every periodic solution $\bar{h}(x, P, L)$ restricted to the interval $[-L, L]$ gives a solution of (2.3a)–(2.3b). And vice versa every solution of (2.3a)–(2.3b) can be extended to the periodic solution $\bar{h}(x, P, L)$ with the least period $T = 2L$.

The asymptotics of the homoclinic solution $\bar{h}(x, P)$ were derived in [23]. If we denote the minimum and the maximum of the homoclinic solution by $h_{\min}(P)$ and $h_{\max}(P)$, respectively, then the minima and maxima of all periodic solutions are bounded by these values. The smallest real root of the algebraic equation $\Pi(h) = P$ is $h_{\min}$. Hence, expanded in ϵ, it is of the form,

$$h_{\min} = \epsilon + \epsilon^2 P + O(\epsilon^3). \tag{2.4}$$

The elliptic center point $h_c(P)$ of (2.3a) is the other real root of $\Pi(h) = P$ and has the asymptotics,

$$h_c = \epsilon(\epsilon P + o(\epsilon P))^{-1/3}. \tag{2.5}$$

Once $h_{\min}(P)$ is determined, the first integral of (2.3a) can be written as

$$\frac{1}{2}\left(\frac{\mathrm{d}\bar{h}}{\mathrm{d}x}\right)^2 = R(\bar{h}), \tag{2.6}$$

where

$$R(\bar{h}) = U\left(\bar{h}\right) - U(h_{\min}) - P(\bar{h} - h_{\min}). \tag{2.7}$$

At the maximum $\bar{h}_x = 0$ and hence $h_{\max}$ is determined by the condition $R(h_{\max}) = 0$ and its asymptotics is

$$h_{\max} = -\frac{U(\epsilon)}{P} + O(\epsilon). \tag{2.8}$$

More detailed asymptotic analysis (see [23]) shows that a stable steady-state solution on $[-L, L]$, i.e., a one-dimensional droplet, can be described by a parabola connected to a thin layer. Then, $h_{\min}$ gives approximately the thickness of this thin layer and $h_{\max}$ is the peak of the droplet.

For the boundary-value problem for the strong-slip model (1.6a)–(1.6b) on the interval $[-L, L]$ we put velocities (or fluxes) at the boundary to zero

$$u = 0 \quad \text{at } x = \pm L. \tag{2.9}$$

i.e., we require conservation of mass (2.2). For the profile $h(x, t)$ we assume that

$$\partial_x h = 0 \quad \text{at } x = \pm L \tag{2.10}$$

as before.

Theorem 2.2 *Steady-state solutions of the system* (1.6a)–(1.6b) *with the boundary conditions* (2.9)–(2.10) *with positive height profile exist and are given by the solutions of* (2.3a)–(2.3b) *and identically zero velocity profile* $\bar{u} \equiv 0$.

Proof The steady states of (1.6a)–(1.6b) are described by

$$\mathrm{Re}\, hu\, \partial_x u = 4\partial_x(h\partial_x u) + h\, \partial_x\, (\partial_{xx} h - \Pi(h)) - \frac{u}{\beta}, \tag{2.11a}$$

$$0 = -\partial_x(hu). \tag{2.11b}$$

From (2.11b) and (2.9) it follows that $hu \equiv 0$. Take any stationary solution $[h(x),\ u(x)]$ with positive height profile. If such a solution exists it follows necessarily

$$u \equiv 0 \text{ for all } x \in [-L,\ L]. \tag{2.12}$$

Substituting (2.12) in (1.6a) one obtains necessarily that $h(x)$ is a solution of (2.3a)–(2.3b) which exists when $P \in (0,\ P_{\max})$ as was shown in [10]. Vice versa, any solution of (2.3a)–(2.3b) determines a stationary solution with identically zero velocity profile for (1.6a)–(1.6b) with the boundary conditions (2.9)–(2.10). □

Remark 2.1 The stationary positive non-constant height profile for (1.6a)–(1.6b) is a solution $\bar{h}(x, P, L)$ of (2.3a)–(2.3b) and hence the asymptotics (2.4)–(2.8) stated for steady states of (1.5) holds for it as well.

2.2 Near-equilibrium solutions

It is well-known that the driving forces that underly the initial dewetting scenario of a thin film, from rupture towards formation of complex fluid patterns, are intermolecular forces. This has been shown in the framework of the no-slip or weak-slip lubrication models; see e.g. [7]. The intermediate- and strong-slip models show similar phases of the initial dewetting scenario, where now interfacial slip has an important influence on the morphology of the resulting patterns and the time scale on which they evolve, see [29,37,38] for a detailed analysis. However, as has been discussed in [23], intermolecular forces are also important in the late phases when arrays of near-equilibrium droplets have formed, connected by a thin layer whose height is determined by the competition between van der Waals attractive and Born repulsive forces. Here, the small flux across this layer plays an important role in the coarsening dynamics of these arrays of droplets, where the central part of each droplet is nearly an equilibrium solution we have just discussed in the previous paragraph.

When Re is sufficiently small, two components of the coarsening regime can be identified [24,32], namely collapse and collision. One can qualitatively explain the driving effects for collapse and collision using the presence of a generalized gradient flow structure. As it is found in [10] the functional

$$E(h) = \int U(h) + \frac{\partial_x^2 h}{2}\, \mathrm{d}x \tag{2.13}$$

is a Lyapunov functional for (1.5) with the boundary conditions (2.1), where $U(h)$ is given by (1.3). Analogously we prove:

Proposition 2.1 *A functional*

$$E(u,h) = \int U(h) + \frac{\mathrm{Re}}{2} h u^2 + \frac{\partial_x^2 h}{2}\,\mathrm{d}x \tag{2.14}$$

is a Lyapunov functional for the system (1.6a)–(1.6b) *with boundary conditions* (2.9)–(2.10) *where* $U(h)$ *is given by* (1.3).

Proof To show that $E(h,t)$ is an energy functional that decreases on the positive solutions of (1.6a)–(1.6b) we establish that $\mathrm{d}E/\mathrm{d}t \le 0$.
We note that by integration by parts and using (2.10), we have

$$\frac{\mathrm{d}E}{\mathrm{d}t} = \mathrm{Re}\int uh\,\partial_t u\,\mathrm{d}x + \int (\Pi(h) - \partial_{xx}h)\,\partial_t h\,\mathrm{d}x + \mathrm{Re}\int \frac{u^2}{2}\,\partial_t h\,\mathrm{d}x. \tag{2.15}$$

Substitution of $\partial_t h$ from (1.6b), integration by parts of the second and third terms and noting the velocity boundary conditions result in

$$\frac{\mathrm{d}E}{\mathrm{d}t} = \mathrm{Re}\int uh\,\partial_t u\,\mathrm{d}x + \int hu\,\partial_x\left(\Pi(h) - \partial_{xx}h\right)\,\mathrm{d}x + \mathrm{Re}\int (hu)u\,\partial_x u\,\mathrm{d}x. \tag{2.16}$$

Recall that from (1.6a)

$$-\partial_x\left(\partial_{xx}h - \Pi(h)\right) = -\mathrm{Re}\left(\partial_t u + u\partial_x u\right) + \frac{4}{h}\partial_x(h\partial_x u) - \frac{u}{\beta h}. \tag{2.17}$$

Using this in (2.16) we obtain

$$\frac{\mathrm{d}E}{\mathrm{d}t} = \int \left(4\partial_x\left(h\partial_x u\right)u - \frac{u^2}{\beta}\right)\mathrm{d}x. \tag{2.18}$$

Integration by parts of the first term and noting (2.9) gives

$$\frac{\mathrm{d}E}{\mathrm{d}t} = -\int 4h\left(\partial_x u\right)^2\,\mathrm{d}x - \int \frac{u^2}{\beta}\,\mathrm{d}x \le 0, \tag{2.19}$$

provided $h(x,t) > 0,\ \forall t > 0$. □

Lyapunov functionals (2.13) and (2.14) also induce a generalized gradient flow structure for (1.7) and (1.6a)–(1.6b), respectively. During the coarsening process in an array of droplets driven by (1.6a)–(1.6b) the energy (2.14) dissipates with the rate given by (2.19). As discussed in detail in [23], in such a framework the collapse component of the coarsening process is driven by the dissipation of energy because the energy of two droplets before collapse is greater than the energy of the remaining one after the collapse of one droplet plus its surrounding thin layer. In turn, migration of droplets can be explained by the presence of the Raleigh principle associated with the generalized gradient structure. It implies the non-zero flux (or velocity) profile between droplets in an array and in fact gives rise for the motion of droplets and consequently for the collision component of the coarsening process. The same description of the two coarsening effects hold for the intermediate-slip case (1.7) with (2.13).

3 Dimension-reduced model for droplet dynamics

3.1 The intermediate-slip case, summary

The description of the slow motion of near-equilibrium droplets in terms of the equilibrium solutions, like those we have just discussed, with parameters characterizing the position of the center of the droplet and its pressure that vary on that slow time scale, was first given in [23] for the no-slip model. Based on their work we briefly illustrate the approach for the intermediate-slip model.

We consider the evolution of one droplet governed by the model (1.7) on the interval $[-L, L]$ at the boundary at which the fluxes

$$J(-L) = J_-, \quad J(+L) = J_+, \tag{3.1}$$

are imposed, where $J_\pm = \sigma \tilde{J}_\pm$ and $\sigma \ll 1$. The fourth-order boundary-value problem is completed by requiring two further boundary conditions

$$h_x(-L) = 0, \quad h_x(L) = 0. \tag{3.2}$$

Since the flux is very small, i.e., of order $\sigma \ll 1$, one can assume the solution $h(x, t)$ (at every fixed time t) to have the form of a perturbed equilibrium droplet solution $\bar{h}$, initially centered at $x = X_0$, corresponding to an initial pressure P_0, i.e., $h(x, 0) = \bar{h}(x - X_0, P_0)$, and evolving on the slow-time scale

$$\tau = \sigma t. \tag{3.3}$$

Following [23] we make the ansatz

$$h(x, \tau) = \bar{h}\,(x - X(\tau), P(\tau)) + \sigma h_1(x, \tau) + O(\sigma^2), \tag{3.4}$$

where the position $X(\tau)$ and the pressure $P(\tau)$ of the droplet vary slowly in time and obtain from (1.7) to leading order in σ

$$-\partial_x \bar{h}\,\frac{\mathrm{d}X}{\mathrm{d}\tau} + \partial_P \bar{h}\,\frac{\mathrm{d}P}{\mathrm{d}\tau} = \mathcal{L}h_1, \tag{3.5}$$

where $\mathcal{L}$ is the differential operator

$$\mathcal{L}h = \partial_x \left(\bar{h}^2 \partial_x \left[\Pi'(\bar{h})h - \partial_{xx}h\right]\right), \tag{3.6}$$

and the perturbation h_1 satisfies boundary conditions (3.2) and flux conditions

$$-\bar{h}^2 \left(\partial_x \left[\Pi'(\bar{h})h_1(-L) - \partial_{xx}h_1(-L)\right]\right) = \tilde{J}_-, \quad -\bar{h}^2 \left(\partial_x \left[\Pi'(\bar{h})h_1(L) - \partial_{xx}h_1(L)\right]\right) = \tilde{J}_+. \tag{3.7}$$

We introduce then formally the adjoint operator $\mathcal{L}^*$,

$$\mathcal{L}^*\psi = (\Pi_x(h) - \partial_{xx}) \left[\partial_x(\bar{h}^2 \partial_x \psi)\right], \tag{3.8}$$

the kernel of which is spanned by two functions

$$\psi_1(x) = 1, \quad \text{and} \quad \psi_2(x) = \int_0^x \frac{\bar{h}(x') - h_{\min}}{\bar{h}(x')^2}\,\mathrm{d}x'. \tag{3.9}$$

Using (3.9) and a suitable change of variables so that the linear problem with nonhomogeneous boundary conditions (3.7) is transformed to one with homogeneous boundary conditions, one can impose two necessary conditions (similar to that used in the Fredholm alternative) on the solvability of (3.5), which result in the system of ODEs for the pressure and position of the droplet, written in the original time scale,

$$\frac{\mathrm{d}P}{\mathrm{d}t} = C_P(P)(J_+ - J_-), \quad \frac{\mathrm{d}X}{\mathrm{d}t} = -C_X(P)(J_+ + J_-), \tag{3.10}$$

where

$$C_P(P) = \frac{1}{-\int_{-L}^{L} \partial_P \bar{h}\,\mathrm{d}x}. \tag{3.11}$$

The only difference to the no-slip case described in [23] is found in the motion coefficient

$$C_X(P) = \frac{\int_{-L}^{L} \frac{\bar{h} - h_{\min}}{\bar{h}^2}\,\mathrm{d}x}{\int_{-L}^{L} \frac{(\bar{h} - h_{\min})^2}{\bar{h}^2}\mathrm{d}x}. \tag{3.12}$$

In Appendix we show that (3.11) and (3.12), along with coefficients for the dimension-reduced model for the strong-slip case in the next section, converge and do not depend on the droplet position $X(t)$.

3.2 Strong-slip case

We again describe the evolution of one droplet on the interval $[-L, L]$ governed now by the system (1.6a)–(1.6b). We restrict our derivation to the regime where

$$\sigma^2 \mathrm{Re} \ll 1, \tag{3.13}$$

i.e., for sufficiently small Re numbers in (1.6a)–(1.6b) and assume again the evolution of the single droplet occurs on a slow time scale τ (3.3) and can be parameterized by the slow evolution of its pressure $P(\tau)$ and position $X(\tau)$. We make the following asymptotic ansatz:

$$\tau = \sigma t \tag{3.14a}$$

$$h(x,t) = \bar{h}(x - X(\tau), P(\tau)) + \sigma h_1(x,\tau) + O(\sigma^2), \tag{3.14b}$$

$$u(x,t) = \sigma u_1(x,\tau) + O(\sigma^2). \tag{3.14c}$$

At the boundary of the interval we impose flux conditions, which can be written in terms of velocity at the boundary:

$$u(\pm L) = \sigma u_{\pm}. \tag{3.15}$$

In this case we define the fluxes $J_{\pm}$ imposed on the droplet as,

$$J_{\pm} = \sigma h_{\min} u_{\pm}. \tag{3.16}$$

After substitution of (3.14b), (3.14c) in (1.6a), (1.6b) and noting (3.13) to the first order in σ we have (in matrix notation)

$$\begin{bmatrix} 0 \\ -\partial_x \bar{h} \frac{\mathrm{d}X}{\mathrm{d}\tau} + \partial_P \bar{h} \frac{\mathrm{d}P}{\mathrm{d}\tau} \end{bmatrix} = \boldsymbol{\mathcal{L}} \begin{bmatrix} h_1 \\ u_1 \end{bmatrix}, \tag{3.17}$$

where $\boldsymbol{\mathcal{L}}$ is the differential operator

$$\boldsymbol{\mathcal{L}} \begin{bmatrix} h \\ u \end{bmatrix} = \begin{bmatrix} 4\,\partial_x(\bar{h}\partial_x u) + \bar{h}\partial_x(\partial_{xx} h - h\Pi'(\bar{h})) - \frac{u}{\beta} \\ -\partial_x(\bar{h}u) \end{bmatrix}. \tag{3.18}$$

The velocity correction term $u_1(x,t)$ satisfies the leading order of (3.15)

$$u_1(\pm L) = u_{\pm}. \tag{3.19}$$

Formally, the adjoint operator to $\boldsymbol{\mathcal{L}}$ is

$$\boldsymbol{\mathcal{L}}^* \begin{bmatrix} g \\ \psi \end{bmatrix} = \begin{bmatrix} 4\partial_x(\bar{h}\partial_x g) - \frac{g}{\beta} + \bar{h}\partial_x \psi \\ \left(\Pi'(\bar{h}) - \partial_{xx}\right)\partial_x(\bar{h}g) \end{bmatrix}. \tag{3.20}$$

It is easy to see that the kernel of the adjoint operator is spanned by two functions,

$$\begin{bmatrix} 0 \\ 1 \end{bmatrix} =: \begin{bmatrix} g_1 \\ \psi_1 \end{bmatrix} \tag{3.21}$$

and

$$\begin{bmatrix} \frac{\bar{h}-h_{\min}}{\bar{h}} \\ \int_0^x \frac{\bar{h}-h_{\min}}{\beta \bar{h}^2} - A(\bar{h}, \partial_{x'}\bar{h}, \partial_{x'x'}\bar{h})\mathrm{d}x' \end{bmatrix} =: \begin{bmatrix} g_2 \\ \psi_2 \end{bmatrix}, \tag{3.22}$$

where

$$A(\bar{h}, \partial_x \bar{h}, \partial_{xx}\bar{h}) = 4\,h_{\min} \frac{\bar{h}\partial_{xx}\bar{h} - \partial_x \bar{h}^2}{\bar{h}^3}. \tag{3.23}$$

Again using (3.21)–(3.22) and transformation of the nonhomogeneous boundary conditions (3.19) to a problem with homogeneous boundary conditions, one can impose two necessary conditions on the solvability of (3.5) which result in the ODEs (3.32a)–(3.32b). Our derivation below is equivalent to this procedure.

To derive an equation for $P(\tau)$ we multiply the second line in the matrix equation (3.17) by ψ_1 and integrate over the interval $[-L, L]$. We can make use of the fact that $\partial_x \bar{h}$ is an odd function and $\int_{-L}^{L} \partial_x(u_1\bar{h})\,\mathrm{d}x = h_{\min}(u_+ - u_-)$. This leads us to the equation

$$\frac{\mathrm{d}P}{\mathrm{d}\tau} = -\left(\int_{-L}^{L} \partial_{\bar{p}}\bar{h}\mathrm{d}x\right)^{-1} h_{\min}(u_+ - u_-), \tag{3.24}$$

which, written in the original time scale, coincides with (3.32a).

Similarly, we multiply the second line in the matrix equation (3.17) by ψ_2 and integrate over the interval $[-L, L]$. Again using odd or even symmetry we get

$$-\frac{\mathrm{d}X}{\mathrm{d}\tau}\int_{-L}^{L} \psi_2\,\partial_x\bar{h}\,\mathrm{d}x = -\int_{-L}^{L} \psi_2\,\partial_x(\bar{h}u_1)\,\mathrm{d}x, \tag{3.25}$$

which transforms to

$$\frac{\mathrm{d}X}{\mathrm{d}\tau} = \frac{\int_{-L}^{L} \psi_2\partial_x(\bar{h}u_1)\mathrm{d}x}{\int_{-L}^{L} \psi_2\partial_x\bar{h}\,\mathrm{d}x}. \tag{3.26}$$

Next we calculate integrals in the denominator and numerator of (3.26). Denote the numerator by

$$I_1 = \int_{-L}^{L} \psi_2\,\partial_x(\bar{h}u_1)\,\mathrm{d}x. \tag{3.27}$$

Then, since $\psi_2(x)$ is an odd function and using (3.22)

$$I_1 = \left[\bar{h}u_1\psi_2\right]_{x=\pm L} - \int_{-L}^{L} (\bar{h}u_1)\partial_x\psi_2\,\mathrm{d}x. \tag{3.28}$$

Using (3.23), integrate by parts and note that $\partial_x\bar{h}|_{x=\pm L} = 0$, this is equal to

$$\begin{aligned} I_1 &= h_{\min}\psi_2(L)(u_+ + u_-) - \int_{-L}^{L} u_1\left(\frac{\bar{h} - h_{\min}}{\beta\bar{h}} - \bar{h}A\right)\mathrm{d}x \\ &= h_{\min}\psi_2(L)(u_+ + u_-) - \int_{-L}^{L} u_1\left(\frac{\bar{h} - h_{\min}}{\beta\bar{h}}\right)\mathrm{d}x + \left[\frac{\partial_x\bar{h}\,h_{\min}}{\bar{h}}u_1\right]_{x=\pm L} - 4\int_{-L}^{L} \frac{\partial_x u_1\,\partial_x\bar{h}\,h_{\min}}{\bar{h}}\,\mathrm{d}x. \end{aligned}$$

Since the third term is zero, making use of the first line from (3.17) and because $\bar{h}|_{x=\pm L} = h_{\min}$ we get

$$\begin{aligned} I_1 &= h_{\min}\psi_2(L)(u_+ + u_-) - \int_{-L}^{L} u_1\left(\frac{\bar{h} - h_{\min}}{\beta\bar{h}}\right)\mathrm{d}x - \left[4\partial_x u_1(\bar{h} - h_{\min})\right]_{x=\pm L} + \int_{-L}^{L} \frac{\bar{h} - h_{\min}}{\bar{h}}\,4\partial_x(\bar{h}u_1)\,\mathrm{d}x \\ &= h_{\min}\psi_2(L)(u_+ + u_-) + \int_{-L}^{L} \frac{\bar{h} - h_{\min}}{\bar{h}}\left(4\partial_x(\bar{h}\partial_x u_1) - \frac{u_1}{\beta}\right)\mathrm{d}x \\ &= h_{\min}\psi_2(L)(u_+ + u_-) - \int_{-L}^{L} (\bar{h} - h_{\min})\partial_x\left(\partial_{xx}h_1 - \Pi'(\bar{h})h_1\right)\mathrm{d}x. \end{aligned}$$

Integrating by parts twice, where we note that $\partial_x \bar{h}|_{x=\pm L} = 0$ and making use of the even property $(\partial_{xx}\bar{h}h_1)|_{x=\pm L} = 0$, we obtain finally

$$I_1 = h_{\min}\psi_2(L)(u_+ + u_-) + \int_{-L}^{L} \partial_x \bar{h}\left(\partial_{xx}h_1 - \Pi'(\bar{h})h_1\right) \mathrm{d}x$$

$$= h_{\min}\psi_2(L)(u_+ + u_-) + \int_{-L}^{L} h_1\left(\partial_{xx} - \Pi'(\bar{h})\right)\partial_x \bar{h}\,\mathrm{d}x = h_{\min}\psi_2(L)(u_+ + u_-). \tag{3.29}$$

Hence, using odd symmetry of $\psi_2(x)$, we can write

$$\int_{-L}^{L} \psi_2\,\partial_x(\bar{h}u)\,\mathrm{d}x = \frac{1}{2}\left(\int_{-L}^{L} \frac{\bar{h} - h_{\min}}{\beta\bar{h}} - \bar{h}A\,\mathrm{d}x\right) h_{\min}(u_+ + u_-). \tag{3.30}$$

The denominator of (3.26) can be written as

$$I_2 := \int_{-L}^{L} \psi_2\,\partial_x \bar{h}\mathrm{d}x = -\int_{-L}^{L} \bar{h}\,\partial_x\psi_2\,\mathrm{d}x + h_{\min}(\psi_2(L) - \psi_2(-L)) = -\int_{-L}^{L} (\bar{h} - h_{\min})\,\partial_x\psi_2\,\mathrm{d}x. \tag{3.31}$$

Using (3.30) and (3.31) where $\psi_2(x)$ is given in (3.22), the evolution equation for the droplet (3.26) written in original time scale, finally takes form

$$\frac{\mathrm{d}P}{\mathrm{d}t} = C_P(P)\,(J_+ - J_-), \tag{3.32a}$$

$$\frac{\mathrm{d}X}{\mathrm{d}t} = -\,C_X(P)\,(J_+ + J_-) \tag{3.32b}$$

for its pressure $P(t)$ and position $X(t)$, where

$$C_P(P) = \frac{1}{-\int_{-L}^{L} \partial_P \bar{h}\,\mathrm{d}x}, \tag{3.33}$$

and the mobility coefficient

$$C_X(P) = \frac{\int_{-L}^{L}\left(\frac{\bar{h}-h_{\min}}{\bar{h}^2} - \beta\,A(\bar{h}, \partial_x\bar{h}, \partial_{xx}\bar{h})\right)\mathrm{d}x}{2\int_{-L}^{L}\left(\frac{(\bar{h}-h_{\min})^2}{\bar{h}^2} - \beta\,A(\bar{h}, \partial_x\bar{h}, \partial_{xx}\bar{h})(\bar{h} - h_{\min})\right)\mathrm{d}x}. \tag{3.34}$$

The coefficients (3.33)–(3.34) depend on the pressure P through the given droplet stationary height profile $\bar{h}(x, P, L)$, its minimum $h_{\min} = \min_x \bar{h}(x, P, L)$ and the function $A(\bar{h}, \partial_x\bar{h}, \partial_{xx}\bar{h})$ defined in (3.23). Next, we provide an asymptotic approximation for the fluxes $J_\pm$ between droplets in an array and finally, arrive to the coupled system of ODEs for them. We observe that (3.34) differs from the corresponding coefficients for no-slip and intermediate slip and depends now on the slip parameter β.

In Appendix we show convergence of the integrals in (3.34). Moreover, we give asymptotics for them in a limit $P,\ \varepsilon \to 0$, which in particular implies that the denominator in (3.34) is positive for all $\beta \geq 0$, but the numerator can change its sign with β. We remark that for the case of negligible Trouton viscosity (when $\beta \to 0$) the function $\beta A(\bar{h}, \partial_x\bar{h}, \partial_{xx}\bar{h}) \to 0$ and we recover the model (3.10)–(3.12) for the intermediate-slip model. On the other hand, when $\beta \to \infty$, we obtain a model for suspended films for which the coefficient (3.34) is replaced by

$$C_X(P) = -\frac{\int_{-L}^{L} A(\bar{h}, \partial_x\bar{h}, \partial_{xx}\bar{h})\,\mathrm{d}x}{2\int_{-L}^{L} A(\bar{h}, \partial_x\bar{h}, \partial_{xx}\bar{h})(\bar{h} - h_{\min})\,\mathrm{d}x}. \tag{3.35}$$

3.3 Approximation for the fluxes between droplets

In order to make use of the reduced models to describe the coarsening process of a whole array of droplets, we derive here asymptotic expressions for the fluxes that a droplet experiences due to its neighboring droplets, again for the intermediate-slip model (1.7) and the strong-slip model (1.6a)–(1.6b).

3.3.1 Intermediate-slip case

As for the no-slip case [23], we note first that the fluxes occur through the thin film of height $h = O(\varepsilon)$, connecting the droplets, which are assumed to have a typical distance of $1/\delta$. Similarly, we obtain expression for the fluxes in the thin film by first scaling the variables to this *inner* region as follows

$$z = \delta x, \quad H = \frac{h}{\varepsilon}, \quad \tau = \sigma t, \tag{3.36}$$

where σ was introduced in (3.14a). For the intermediate-slip case it can be taken as

$$\sigma = \varepsilon^2 \delta. \tag{3.37}$$

Substitution of (3.36) in (1.7) yields

$$\varepsilon^2 \delta^{-1} H_\tau = \partial_z \left(H^2 \partial_z (\mathcal{U}'(H) - \varepsilon^2 \delta^2 \partial_{zz} H) \right), \tag{3.38}$$

with $\mathcal{U}(H) := U(h/\epsilon)$. Hence, assuming that $\varepsilon^2/\delta \ll 1$, to the leading order the quasi stationary problem is

$$0 = \partial_{zz}[\mathcal{V}(H)], \tag{3.39}$$

where $\mathcal{V}(H)$ is defined by

$$\frac{\mathrm{d}\mathcal{V}}{\mathrm{d}H} = H^2 \frac{\mathrm{d}^2 \mathcal{U}}{\mathrm{d}^2 H} \text{ which is, in unscaled variables } \frac{\mathrm{d}V}{\mathrm{d}h} = h^2 \frac{\mathrm{d}^2 U}{\mathrm{d}h^2}, \tag{3.40}$$

and $V(h) = \varepsilon \mathcal{V}(h/\varepsilon)$, so that the flux between droplets is $J = -\partial_x V(h)$.

Solving the *outer* boundary-value problem $\partial_{xx} V(h) = 0$ with $V = V(h_{\min})$ at the apparent contact line, i.e., where the droplet merges into the thin film, we observe that as in [23] for the no-slip case, also here we obtain that the flux between two neighboring droplets, labeled by k and $k+1$, is constant and given by their positions and pressures as

$$J_{k,k+1} = -\frac{V(h_{\min}(P_{k+1})) - V(h_{\min}(P_k))}{[X_{k+1} - w(P_{k+1})] - [X_k + w(P_k)]}. \tag{3.41}$$

The main difference with the no-slip case is the difference in the mobility and hence the regime of quasistatic behavior. Furthermore, in contrast to (1.1), for the intermediate-slip we now have

$$V = \frac{3\varepsilon^2}{h} - \frac{2\varepsilon^3}{h^2}. \tag{3.42}$$

3.3.2 Strong-slip case

As we did throughout the paper, we neglect the inertial terms in the strong-slip model to obtain

$$0 = \frac{4}{h} \partial_x (h \partial_x u) + \partial_x \left(\partial_{xx} h - \Pi(h) \right) - \frac{u}{\beta h}, \tag{3.43a}$$

$$\partial_t h = -\partial_x (hu). \tag{3.43b}$$

In addition to (3.36) we set $W = \gamma u$, i.e., we introduce the scalings for the *inner* variables as

$$z = \delta x, \quad H = \frac{h}{\varepsilon}, \quad \tau = \sigma t, \quad W = \gamma u. \tag{3.44}$$

The equations in these *inner* scalings are

$$0 = \frac{\varepsilon\delta}{\gamma}\frac{4}{H}\partial_z(H\partial_z W) + \partial_z\left(\varepsilon^2\delta^2\partial_{zz}H - \mathcal{U}'(H)\right) - \frac{1}{\delta\gamma}\frac{W}{\beta H}, \tag{3.45a}$$

$$\frac{\sigma\gamma}{\delta}\,\partial_\tau H = -\,\partial_z\,(HW), \tag{3.45b}$$

where

$$\Pi(\varepsilon\, H) = \frac{1}{\varepsilon}\left(\frac{1}{H}\right)^n\left[1-\left(\frac{1}{H}\right)^{m-1}\right] = \frac{1}{\varepsilon}\,\mathcal{U}'(H). \tag{3.46}$$

In the film between the droplets the most important term is the intermolecular potential $\mathcal{U}$ and surface tension should be negligible. Additionally, as for the no-slip and intermediate slip cases, we consider only the situation with constant flux, i.e., in the following balances of terms we assume that the rate of change in H vanishes, so that $\sigma\gamma/\delta \ll 1$. If we assume that the fluxes between the droplets will set the time scale, then, since

$$J = uh = \frac{\varepsilon}{\gamma}WH \quad \text{we get with } J = \sigma\mathcal{J} \text{ and } \mathcal{J} = WH \quad \text{the relation } \gamma = \frac{\varepsilon}{\sigma}. \tag{3.47}$$

This means, that requiring constant flux amounts to the regime $\varepsilon/\delta \ll 1$. We consider here the case, where the slip term enters the leading-order equation, i.e.,

$$\frac{1}{\delta\gamma} \sim 1 \quad \text{so that } \sigma = \varepsilon\delta, \tag{3.48}$$

and the Trouton viscosity and the surface-tension terms, which are then $O(\varepsilon\delta^2)$ and $O(\varepsilon^2\delta^2)$, respectively, are neglected. The leading-order equations for this case are

$$0 = \beta H^2\partial_z\left(\mathcal{U}'(H)\right) + HW, \tag{3.49a}$$

$$0 = \partial_z\,(HW), \tag{3.49b}$$

This implies that

$$HW = -\beta H^2\partial_z\left(\mathcal{U}'(H)\right) \tag{3.50}$$

and used in (3.49b) we obtain

$$0 = \partial_z\left(H^2\partial_z\left(\mathcal{U}'(H)\right)\right). \tag{3.51}$$

If we define $\mathcal{V}(H)$ as in the intermediate-slip case and note that in *outer* scales

$$\partial_x V = \frac{\mathrm{d}V}{\mathrm{d}h}\partial_x h = h^2\frac{\mathrm{d}^2U}{\mathrm{d}h^2}\partial_x h, \tag{3.52}$$

we can express the flux as

$$J = uh = -\beta h^2\frac{\mathrm{d}^2U}{\mathrm{d}h^2}\partial_x h = -\beta\partial_x V. \tag{3.53}$$

Integrating, we can solve for V and obtain the same expression as in (3.42).

A comparison of the predictions of the lubrication model with the corresponding ODE model for the strong-slip case above, is illustrated in Fig. 1. Here we follow the evolution of the array of droplets and observe good agreement except for the actual collapse events.

Finally, note that if we rescale the velocity or flux (3.53) by β, $J = \beta J_{IS}$, where J_{IS} denotes the flux in the intermediate-slip case, and the time in (3.32a), (3.32b) by $1/\beta$, then we recover the ODE model for the intermediate-slip case in the limit $\beta \to 0$. Moreover, our preliminary asymptotic studies, as well as numerical simulations, suggest that further constant-flux regimes, for which the model (3.32a)–(3.34) remains valid, are possible for large β. Their complete asymptotic investigation as well as their implications on the coarsening dynamics and rates is subject of an upcoming paper.

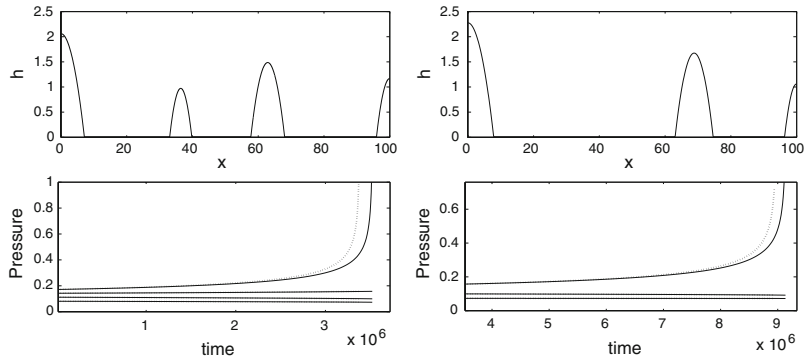

Fig. 1 Comparison of the results of the ODE model(*dotted line*) and the lubrication model (*solid line*) for the strong-slip case. Shown are the evolution of droplet pressures until collapse of the second droplet (*left*), and until the collapse of the fourth droplet (*right*) with $\beta = 1$, $\varepsilon = 0.01$, $L = 100$, $\mathrm{Re} = 0$. *Upper row* shows the initial conditions for each collapse event

4 Coarsening dynamics for increasing slip lengths

4.1 Numerical methods

The numerical methods used in the preceding section and the following section are now briefly described. For the numerical treatment of the lubrication models we used the scheme, developed in [29,39] with D. Peschka and A. Münch [37]. It solves the lubrication models (1.1), (1.7) and (1.5) with the boundary conditions (2.1), and the strong-slip model (1.6a)–(1.6b) with the boundary conditions (2.9)–(2.10). It is a fully implicit finite-difference scheme on a general nonuniform mesh in space with adaptive time step. At every time step the nonlinear system of algebraic equations is solved using Newton's method. At every Newton iteration the resulting linear system of algebraic equations is solved using LAPACK library.

The numerical solutions for the ODE models for the intermediate- and strong-slip models, i.e.,

$$\frac{\mathrm{d}P_k}{\mathrm{d}t} = C_P(P_k)(J_{k+1,k} - J_{k,k-1}), \quad \frac{\mathrm{d}X_k}{\mathrm{d}t} = -C_X(P_k)(J_{k+1,k} + J_{k,k-1}) \tag{4.1}$$

where $C_P(P_k)$ and $C_X(P_k)$ are given by (3.11) and (3.12), respectively, for the intermediate-slip model and (3.11) and (3.34), for the strong-slip model were obtained using a fourth-order adaptive time step Runge–Kutta method in Matlab. The main difficulty was to calculate numerically the coefficients (3.11), (3.12) and (3.34). The algorithm of their integration is explained in Appendix.

4.2 New coarsening effects

The numerical simulations of the lubrication models all confirmed the formation and the existence of coarsening behavior for arrays of near-equilibrium droplets. We find that, while there are mainly quantitative differences for the coarsening process for the intermediate-slip model in comparison to the known no-slip case, for the strong-slip case some qualitative new effects of the coarsening process can be observed which do not have counterparts for the no- and intermediate-slip models.

For negligible inertial terms and β of small to $O(1)$ magnitude we show the existence of a critical value of the slip parameter (4.6) at which the direction of the droplet migration changes. This and its consequences are investigated numerically and analytically in Sect. 4.3.

Moreover, it was shown in [23,24] that in contrast to the Cahn–Hilliard equation, used to describe coarsening processes such as phase separating binary alloys, the lubrication models describing coarsening arrays of droplets demonstrate besides Ostwald ripening, i.e., droplet collapse, the existence of collisions of droplets as another coarsening mechanism. So far this component was known to be comparable with collapse only for the no-slip model.

It was shown in [32] for the lubrication model (1.5) with mobility $M(h) = h^q$, $q > 0$, that the collision component is negligible for $q < 3$ and saturates for $q > 3$ becoming comparable with collapse. That means that for the intermediate-slip case (1.7) the collision component of the coarsening process is negligible, while for the no-slip case it is larger and comparable to the collapse component, but nevertheless it saturates for $q > 3$. In contrast we will show in Sect. 4.4, that in the strong-slip case the collision component continuously increases and eventually becomes dominant as β increases.

4.3 Slippage as a control parameter for migration

One of the characteristic properties of the weak-slip model (1.5) along with (1.1) and (1.7) is the following fact: the droplet migrates always opposite to the effective applied flux; see in particular the detailed discussion in [32]. In the case of the kth droplet in the array of N droplets the effective flux applied on it is

$$J_{eff} = J_{k+1} + J_{k-1}. \tag{4.2}$$

The explanation of the property is straightforward from the migration equation (3.10) and the expression for the motion coefficient (3.12). One observes that the integrands of numerator and denominator of (3.12) are always positive because $\bar{h}(x, P) > h_{\min}$ for all x and P and hence $C_X(P) > 0$. Then from (3.10) it follows that the sign of $\mathrm{d}X/\mathrm{d}t$ is always opposite to the sign of (4.2).

In contrast, in the case of the strong-slip model the analysis of (3.32b) and (3.34) shows that a droplet can migrate opposite or in the same direction of the applied effective flux (4.2), depending on the value of the slippage parameter β. This fact is explained by the influence of the new term in the expression for (3.34), which is connected with the presence of the Trouton viscosity term in the system (1.6a)–(1.6b).

Proposition 4.1 *When ε and the pressure P of the droplet are sufficiently small, there exist a unique zero $\beta = \beta_{\mathrm{crit}}(P, \varepsilon) \ll 1$ of (3.34) as a function of β, which has the asymptotics:*

$$\beta_{\mathrm{crit}} = K\varepsilon \log\left(\frac{2}{3\varepsilon P}\right) + o(\varepsilon); \tag{4.3}$$

and such that the direction of the droplet migration is opposite (in the same direction as) the flux when $\beta < \beta_{\mathrm{crit}}$ ($\beta > \beta_{\mathrm{crit}}$).

Proof In Appendix we derive the asymptotic representations (A.20) and (A.19) for the integrals

$$I_{2,m} = \int_{-L}^{L} A(\bar{h}, \partial_x\bar{h}, \partial_{xx}\bar{h})(\bar{h} - h_{\min})^m \,\mathrm{d}x \tag{4.4}$$

and the approximation (A.15) for the integral

$$I_{1,1} = \int_{-L}^{L} \frac{(\bar{h} - h_{\min})}{\bar{h}^2} \,\mathrm{d}x, \tag{4.5}$$

as $\varepsilon,\ P \to 0$. The expression (A.20) shows that the integral $I_{2,1}$ is negative for sufficiently small ε and P. This in turn implies that the denominator of the mobility coefficient (3.34) is positive. The second expression shows that the integral $I_{2,0}$ is positive for sufficiently small ε and P. From this and the fact that integral $I_{1,1}$ is positive, because $\bar{h} > h_{\min} > 0$, existence and uniqueness of β_{crit} follows and it is given as

$$\beta_{\mathrm{crit}} := \frac{\int_{-L}^{L} \frac{\bar{h} - h_{\min}}{\bar{h}^2} \,\mathrm{d}x}{\int_{-L}^{L} A(\bar{h}, \partial_x\bar{h}, \partial_{xx}\bar{h}) \,\mathrm{d}x}. \tag{4.6}$$

This definition together with (A.15) and (A.19) for the integrals $I_{1,1}$ and $I_{2,m}$ imply (4.3). □

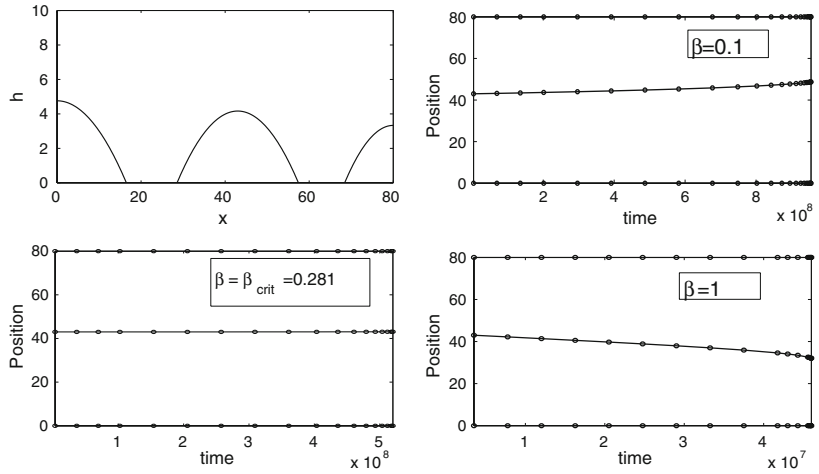

Fig. 2 Migration of the middle droplet in the array of three droplets (*upper-left plot*) for different β. $L = 80, \epsilon = 0.01, \mathrm{Re} = 0, P_2 = 0.4$

This migration effect is illustrated in Fig. 2. For a given array of three droplets β_{crit} for the middle one was calculated and then solutions of (3.32a), (3.32b) with three different values for the slip parameter $\beta_1 < \beta_2 = \beta_{\mathrm{crit}} < \beta_3$ were obtained. Note that in the case $\beta = \beta_{\mathrm{crit}}$ the middle droplet almost does not move. Using the formula (3.41) and given parameters of the droplet array one can calculate that the effective flux applied on the middle droplet is always negative. So in the case $\beta < \beta_{\mathrm{crit}}$ it moves opposite to the flux and in the case $\beta > \beta_{\mathrm{crit}}$ in the same direction of the flux.

Additionally, we recall that for the no-slip model it was shown in [24] that collisions are typically observed for a system of at least three droplets, when two bigger droplets are attracted by a smaller droplet in between. For the strong-slip model (1.6a)–(1.6b) two-droplet collisions are typically admitted when $\beta > \beta_{\mathrm{crit}}$. An example of a two-droplet collision is shown in Fig. 3 with $\beta = 1$. It is a direct consequence of the fact that a droplet can migrate in the same direction as the flux. We remark that in the case $\beta < \beta_{\mathrm{crit}}$ (see Fig. 3 with $\beta = 0.1$) the two-droplet collision is not possible and the strong-slip model behaves just as (1.7).

4.4 Coarsening patterns for increasing slippage

In this section we consider the modeling example from [24] of a coarsening process involving initially ten droplets [24, Figs. 1 and 10] and look how the coarsening scenario changes with slippage in comparison to the no-slip case analyzed in the latter article. Starting from an initial array of ten droplets as shown in Fig. 4 we follow the paths of the first eight droplets in time in Fig. 5, where we vary slippage while keeping $\varepsilon = 0.1$ fixed. Beginning with the intermediate-slip regime and increasing slippage for the strong-slip regime we observe several changes in coarsening behavior, first due to the existence of β_{crit} for every droplet in the array and second (also as a consequence of the first fact) that migration and hence collision rates change with slippage in comparison with collapse.

For every droplet in the array with initial pressure P_j one can calculate $\beta_{\mathrm{crit},j} = \beta_{\mathrm{crit}}(P_j)$. In the example we chose, the values for $\beta_{\mathrm{crit},j}$ do not differ much from each other and are approximately contained in the interval $I = ([1.18, 1.3])$. When slippage is below 1.18, all droplets move opposite to the flux, but the value of their mobility coefficient in the reduced ODE goes to zero and hence migration rates also approach zero as β is increased. This effect can be seen in Fig. 5 for $\beta = 0.3$ and $\beta = 0.5$. In the former case the first two coarsening effects are the same as for the intermediate-slip case, namely first collapse of the 6th droplet and then collision of the 2nd and 3rd ones. But in the case $\beta = 0.5$ migration becomes so slow that the 2nd and the 3rd drops can not collide, instead the former one collapses first.

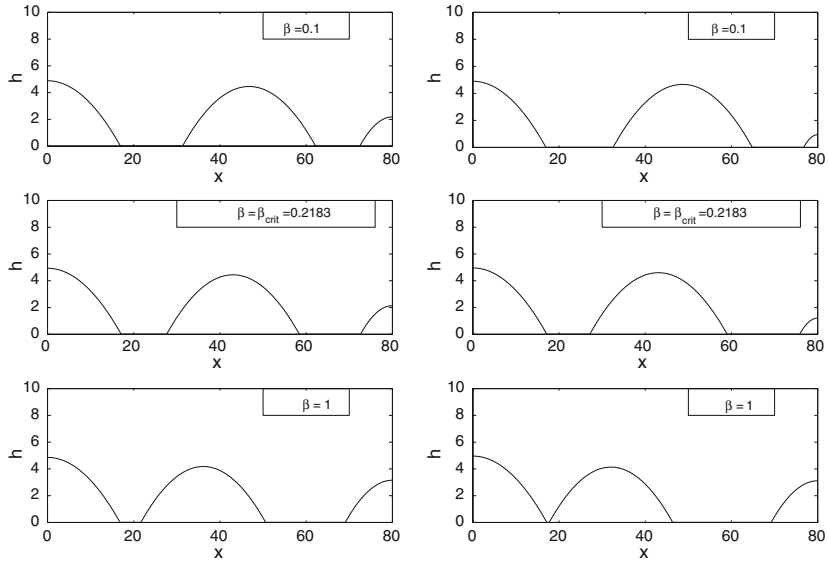

Fig. 3 The evolution of three droplets for three different β with initial profile and parameters as in Fig. 2. The *first and second column* correspond to middle and the end of the evolution of the droplets, respectively

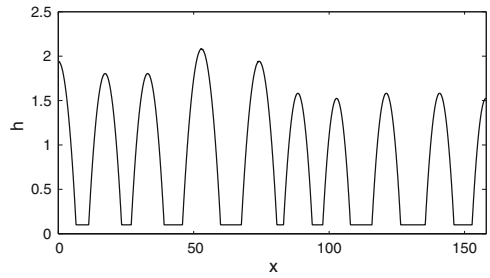

Fig. 4 Initial profile used for all the coarsening simulations in Fig. 5

The next qualitative change in the coarsening behavior occurs when passing the critical interval I. We observe that one droplet after another change their migration direction from opposite to the flux to the same direction of the flux. For example in the case $\beta = 1.25$ smaller droplets (like the 2nd, 3rd, 6th and 7th) have already changed their migration direction, but the bigger ones not. Nevertheless, we do not observe any change in coarsening events in comparison with the case $\beta = 0.5$.

To see new events we need to increase slippage further. As a consequence the migration coefficients in the reduced model increase and hence the migration rates. This, together with the fact that now all droplets migrate in the same direction as the flux, considerably changes the coarsening events in our example. For example, when $\beta = 2$ we see that both the 5th and 6th droplets migrate to the left, before they moved to each other together with the 4th which now migrates to the right. Moreover, the 2nd and 3rd droplets do not attract each other anymore, rather, the former one collides with the first droplet and this becomes the second coarsening event in our system. The first one is collapse of the 6th droplet.

Increasing slippage even higher, here up to $\beta = 3.5$, we see that migration rates increase further, so that now the 4th and 5th droplet collide (first coarsening event now) before the 1st and 2nd ones and before the 6th collapses (second coarsening event). In principle one could increase slippage further, so that one after the other coarsening event changes from collapse to collision.

In summary we demonstrated that increasing slippage, here in the interval $[0,\ 3.5]$, several different coarsening behaviors for an initial droplet array can be distinguished. They illustrate that the existence of β_{crit} influences the

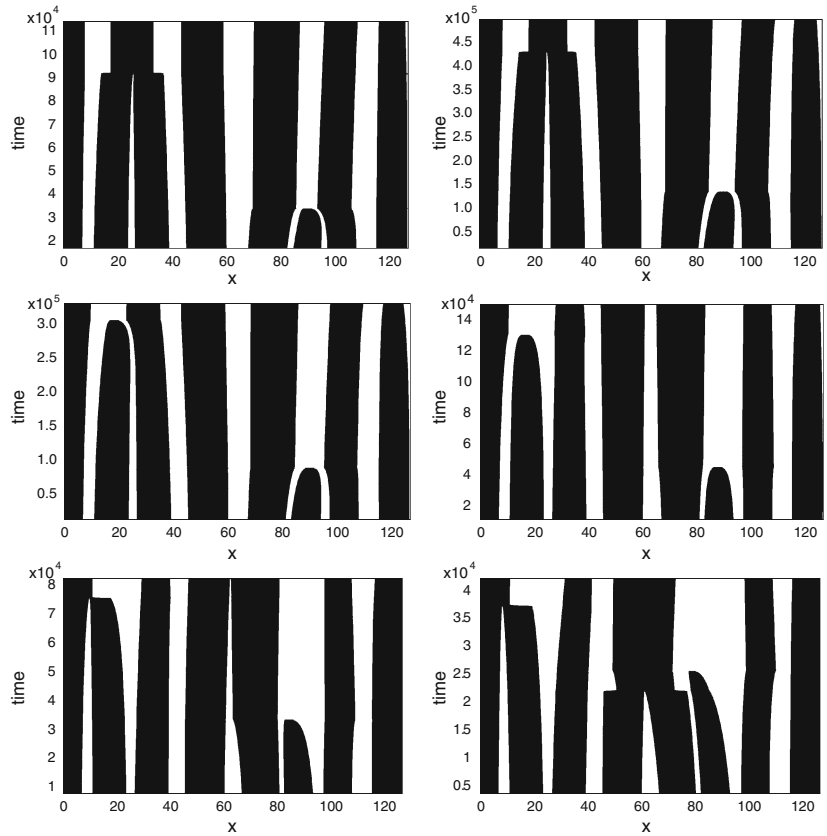

Fig. 5 First two coarsening events in the initial array of 8 droplets for 6 different slip values: Intermediate-slip model, strong-slip model with $\beta = 0.3$, $\beta = 0.5$, $\beta = 1.25$, $\beta = 2$, $\beta = 3.5$ (arranged from *left to right* and from *top to bottom*). The *black* part of the pattern denotes the support of the droplets

coarsening dynamics by changing the direction of migration, migration rates, which decrease to zero when one approaches the critical slippage interval I and that collisions become dominant after further increase of the slip length.

4.5 Coarsening rates

As was shown in previous sections the value of the slip-length parameter β in the strong-slip regime considerably influences the coarsening behavior of an initial system of droplets and the contribution of collision component depending on how close this value is to the mean critical slip length of the system (at which all droplets almost do not move and just collapse). Naturally, this fact should imply some dependence of the collision-dominated coarsening rates on the value of the slip length.

In [23] the coarsening dynamics of initially well-separated systems of droplets which experience in general only collapse-coarsening effects (so called collapse-dominated coarsening rates) was investigated and it was shown that the statistical number of droplets $N(t)$ in such a system changes in time according to

$$N(t) \propto t^{-2/5}. \tag{4.7}$$

Furthermore, reference [33] considered the lubrication model (1.5) with mobility term $M(h) = h$ and derived the law (4.7) on the basis of the gradient flow structure of the equation. As the equation for the evolution of droplet pressures is the same in the reduced models for all slip-regimes, it is natural to expect that the coarsening rate law

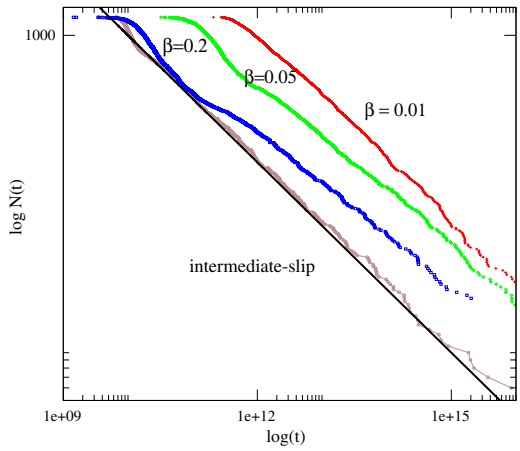

Fig. 6 Coarsening rates for the intermediate-slip regime, strong-slip regime with $\beta = 0.2$, $\beta = 0.05$ and $\beta = 0.01$. The *solid line* shows $t^{-2/5}$ and agrees well with the coarsening rate for the intermediate-slip regime, as it should. This behavior is approached again as $\beta \to 0$

for collapse-dominated systems does not depend on the chosen slip regime and is always given by (4.7). Moreover, in [24] it was shown that for the 1D no-slip regime any initial system of droplets will coarsen according to (4.7) independent of the proportional number of collision and collapse events during the coarsening process.

We simulated for various initial configurations and number of droplets N the coarsening dynamics of the intermediate-slip regime and found (as was expected from the results of [32]) that the percentage of collisions is very small. As is claimed in [32], the intermediate-slip regime is essentially collapse-dominated and hence coarsening rates for it are given by (4.7).

We then solved the reduced system (3.32a), (3.32b) for the corresponding strong-slip model for the similar initial distributions of droplets and values for the slip-length parameter $\beta = 0.2$, $\beta = 0.05$ and $\beta = 0.01$ using all times the flux approximation (3.53) with (3.42). We observed firstly that the proportion of collisions becomes dominant and increases with slippage. Secondly, the corresponding coarsening rates have slopes $\sim t^{-1/3}$ for $\beta = 0.2$ and decrease to $\sim t^{-2/5}$ as shown in Fig. 6. Note, that for the chosen parameters ε and P_{mean} the formula (4.3) entails that the mean critical slip-length parameter $\beta_{\text{crit}} \approx 0.01$ and our chosen slip lengths $\beta = 0.05$, $\beta = 0.2$ are beyond the critical values.

The analytical derivation and more precise analysis for the dependence of collision-dominated coarsening rates on the slip length in the strong-slip regime is subject of our ongoing research.

5 Conclusions

We have derived reduced models that capture the slow-time migration of arrays of droplets driven by intermolecular forces and analysed the influence of interfacial slippage. We distinguished several new qualitatively different coarsening behaviors as the slip length is increased. Apart from the no-slip and intermediate-slip case, also the strong-slip case shows migration direction of a droplet opposite to the flux, but for this case only below a critical slip length β_{crit}. At this value the droplet will stop moving, and above this value the droplet will migrate in the same direction as the flux. In future work, it would be interesting to examine the physical reason behind this change of direction of migration. Certainly, it is connected with the additional Trouton-viscosity term, which may yield a restoring stress in the lateral direction in the film connecting the droplets.

Along with this transition also the occurrence of the coarsening mechanisms, i.e., collapse and collision, change. While for the no-slip, intermediate-slip and for the strong-slip case until the critical slip length, the collision component becomes at most comparable to collapse, increasing slippage beyond β_{crit} collision component becomes dominant. Additionally, the type of collision also changes; below β_{crit} it typically takes at least three droplets for a collision event, where the smaller droplet in the middle vanishes. Above β_{crit} collisions of just two droplets are typical owing to the fact that now the droplets move in the same direction as the flux.

As a result of these different coarsening behaviours we have also illustrated that the coarsening patterns will take completely different paths as the slip length is increased.

Interestingly, the experimental results by [14,15] for a system of copolymer (PS $-$ b $-$ PMMA) dewetting autophobically from a layer of molecular brushes that coat a substrate (SiO_2/Si), suggest that collisions of droplets to be the cause of coarsening. Since these experimental studies are the only ones on this topic that we are aware of, it would be interesting to revisit a system such as in [28], where we have already demonstrated the impact of slippage in the early stages of the dewetting process. For the late stages one could compare coarsening rates as a function of slippage by using different hydrophobic coatings such as used in [28]. Our present analysis would have to be extended to the three-dimensional case.

All of the cases considered in this paper neglect inertial effects and the limiting cases of very large β. Comparison with numerical solutions of the strong-slip lubrication model show that, if (3.13) is no longer satisfied, the approximations (3.11) and (3.34) cease to be valid for (1.6a)–(1.6b). Additionally, our preliminary numerical investigations show that for example when $\sigma^2 \mathrm{Re} = O(1)$, then qualitatively new droplet dynamics can be identified. The pressures inside the droplets are no longer constant and have a complicated nonlinear structure. The two components of the coarsening process, collision and collapse, still exist, but now also oscillatory behavior of droplet formation appears. The question arises if for regimes, where $\sigma^2 \mathrm{Re} \gg O(1)$, it is still possible to obtain reduced models for the late phases of dewetting. This is subject of our ongoing studies.

Acknowledgements The authors thank Lutz Recke, Andreas Münch and Dirk Peschka for many fruitful discussions. GK gratefully acknowledges support from the DFG Graduate Training Program 1128 "Analysis, Numerics and Optimization". BW gratefully acknowledges funding by the DFG Research Center MATHEON.

Appendix: convergence, numerical integration and asymptotics for the coefficients $C_P(P)$ and $C_X(P)$

Here we show that the coefficient functions in (3.11), (3.12), (3.33) and (3.34) converge and can be integrated numerically. Below K_i, $i = 1, \ldots, 11$ everywhere denote constants.

The contribution to the coefficient $C_P(P)$ to the leading order comes from the droplet core and we can neglect the contribution from the ultrathin film when $\epsilon \ll 1$. Therefore it can be calculated as in [23]:

$$C_P(P) = \frac{1}{-\int_{-L}^{L} \partial_P \bar{h}\, \mathrm{d}x} = \frac{3P^3}{4A^3}, \tag{A.1}$$

where $A = -\sqrt{2|U(\epsilon)|}$ is a droplet contact angle (see [23]).

For the coefficient $C_X(P)$ we have the formulas (3.12) or (3.34) which can be written as ratios of improper integrals. In order to prove that these integrals converge, we need to prove that the integrals

$$I_{1,n} := \int_{-L}^{L} \frac{(\bar{h} - h_{\min})^n}{\bar{h}^2}\, \mathrm{d}x, \quad I_{2,m} := \int_{-L}^{L} A(\bar{h}, \partial_x \bar{h}, \partial_{xx} \bar{h})(\bar{h} - h_{\min})^m\, \mathrm{d}x \tag{A.2}$$

converge for all $P \in (0, P_{\max})$, where $n = 1, 2$ and $m = 0, 1$.

Let us start from $I_{1,n}$. Using first integral $R(h)$ given by (2.7) for the steady state equation (2.3a) one can change variables in (A.2) and integrate both integrals over $h_{\min} \le h \le h_{\max}$:

$$I_{1,n} = 2 \int_{h_{\min}}^{h_{\max}} \frac{(h - h_{\min})^n}{h^2 \sqrt{2R(h)}}\, \mathrm{d}h. \tag{A.3}$$

These integrals are improper at both ends of the integration interval because $R(h_{\min}) = R(h_{\max}) = 0$. One can see that $R(h)$ is of a form:

$$R(h) = \frac{K_1 (h - h_{\min})^2 (h - h_{\max})(h - h_{\mathrm{neg}})}{h^3}, \tag{A.4}$$

where $h_{\text{neg}} < 0$ is the third real root of $R(h)$. Canceling $h - h_{\min}$ in the denominator and the numerator, the integral becomes improper only at the end $h_{\max}$

$$I_{1,n} = K_2 \int_{h_{\min}}^{h_{\max}} \frac{(h - h_{\min})^{n-1}}{\sqrt{h(h - h_{\max})(h - h_{\text{neg}})}} \, \mathrm{d}h, \tag{A.5}$$

We assure that $I_{1,n}$ converges by making a second change of variables in (A.5):

$$h = h_{\max} \cos(\theta). \tag{A.6}$$

Then we find from (A.5)

$$I_{1,n} = K_3 \int_0^{\operatorname{acos}\left(\frac{h_{\min}}{h_{\max}}\right)} \frac{(\cos(\theta) - h_{\min}/h_{\max})^{n-1} \cos(\theta/2)}{\sqrt{\cos(\theta)(\cos(\theta) - h_{\text{neg}}/h_{\max})}} \, \mathrm{d}\theta. \tag{A.7}$$

The last integral is proper and can be integrated by the three-point Gaussian quadrature.

Let us now calculate the second type of integrals, namely $I_{2,m}$ in (A.2). As before we use (2.7) to change variables and integrate over $h_{\min} \le h \le h_{\max}$:

$$\begin{aligned} I_{2,m} &= 2 \int_{h_{\min}}^{h_{\max}} \frac{A(h, \partial_x h, \partial_{xx} h)(h - h_{\min})^m}{\sqrt{2R(h)}} \mathrm{d}h \text{ (using (3.23), (2.3a)–(2.3b) and (2.7))} \\ &= 8 \int_{h_{\min}}^{h_{\max}} \frac{h_{\min}(h - h_{\min})^m (\Pi(h) - P)}{h^2 \sqrt{2R(h)}} \mathrm{d}h - 8 \int_{h_{\min}}^{h_{\max}} \frac{h_{\min} \, (h - h_{\min})^m \sqrt{2R(h)}}{h^3} \mathrm{d}h. \\ &=: 8 h_{\min} \left(I_{2,m}^1 + I_{2,m}^2 \right) \end{aligned} \tag{A.8}$$

The second integral $I_{2,m}^2$ in (A.8) is a proper integral at both ends of the integration interval and therefore converges. But the first integral $I_{2,m}^1$ is improper at the both ends. Note that numerator $\Pi(h) - P$ is of the form

$$\Pi(h) - P = \frac{K_4 (h - h_{\min})(h - h_c)(h^2 + a^2)}{h^4}, \tag{A.9}$$

where h_c is given by (2.5) in Sect. 2 and a^2 is the modulus of two conjugate complex roots of $\Pi(h) = P$. Using (A.4) and (A.9) one can simplify $I_{2,m}^1$ as follows:

$$I_{2,m}^1 = K_5 \int_{h_{\min}}^{h_{\max}} \frac{(h - h_{\min})^m (h - h_c)(h^2 + a^2)}{\sqrt{h^9 (h - h_{\max})(h - h_{\text{neg}})}} \mathrm{d}h. \tag{A.10}$$

Hence $I_{2,m}^1$ becomes proper at $h_{\min}$. To make it proper at the right end $h_{\max}$ we use again trigonometric change of variables (A.6) and proceed exactly as in case of $I_{1,n}$ above. It makes $I_{2,m}^1$ a proper integral that can be integrated by the three-point Gaussian quadrature.

We have in summary that both integral in (A.2) converge (in particularly does not depend on $X(t)$) and can be calculated numerically. The numerical error of the calculation of (3.12) or (3.34) is algebraic in ϵ due to the usage of truncated expansions (2.4) and (2.8) in powers of ϵ for $h_{\min}$ and $h_{\max}$, respectively.

Besides the direct calculation of (A.2) one can estimate these integrals asymptotically in a limit $P, \epsilon \to 0$ following the similar approach in [24, Appendix]. Such asymtotics we use in the Sect. 4.2 for estimating of β_{crit}. For such purposes we derive here the leading-order asymptotics of integrals $I_{1,1}$ and $I_{2,0}$ and prove that $I_{2,0} > 0$ and $I_{2,1} < 0$ for all sufficiently small P and ϵ.

Applying the Taylor expansion to (2.7) in the neighborhoods of $h_{\min}$ and $h_{\max}$ one can obtain:

$$R(h) \sim \begin{cases} \frac{1}{2}U''(h_{\min})(h-h_{\min})^2, & h \to h_{\min} \\ \left[P - U'(h_{\max})\right](h_{\max}-h), & h \to h_{\max} \end{cases}, \tag{A.11}$$

Analogously one can show:

$$\Pi(h) - P \sim \Pi(h_{\min})(h-h_{\min}), h \to h_{\min}. \tag{A.12}$$

To estimate $I_{1,1}$, from (A.11) we note that for $h \to h_{\min}$ the ratio $(h-h_{\min})/\sqrt{2R(h)}$ approaches a positive constant. Consequently, for $h_{\min} \to 0$, the factor $1/h^2$ makes the integrand relatively large there. This contribution, along with the contribution for $h \to h_{\max}$ leads to the estimate,

$$I_{1,1} \approx \frac{1}{\sqrt{U''(h_{\min})}} \int_{h_{\min}}^{h_c} \frac{\mathrm{d}h}{h^2} + \frac{1}{\sqrt{2|P-U'(h_{\max})|}} \int_{h_{\min}}^{h_{\max}} \frac{h-h_{\min}}{h^2\sqrt{h_{\max}-h}}\mathrm{d}h \tag{A.13}$$

where h_c given by (2.5) yields an effective cut-off for the influence of the behavior near $h_{\min}$. Both integrals in (A.13) can be integrated analytically. Denoting them $I^1_{1,1}$ and $I^2_{2,1}$, respectively, and expanding w.r.t. $P, \epsilon \to 0$ one obtains to leading order:

$$I^1_{1,1} \approx K_6 + O(\epsilon P); \quad I^2_{1,1} \approx K_7 \log\left(\frac{2}{3\epsilon P}\right) + K_8 + O(\epsilon P), \tag{A.14}$$

Hence the final asymptotics for $I_{1,1}$ w.r.t. $P, \epsilon \to 0$ is of the form:

$$I_{1,1} \approx K_7 \log\left(\frac{2}{3\epsilon P}\right) + O(1) \tag{A.15}$$

Let us now estimate the integral $I_{2,0}$. To this end one needs to estimate integrals $I^1_{2,0}$ and $I^2_{2,0}$ in (A.8). For the integral $I^1_{2,0}$ analogously to (A.13) and using (A.11), (A.12) and relation between (1.2), (1.3) from the Sect. 1 one can write

$$I^1_{2,0} = \int_{h_{\min}}^{h_{\max}} \frac{\Pi(h)-P}{h^2\sqrt{2R(h)}}\mathrm{d}h \approx \sqrt{\Pi'(h_{\min})} \int_{h_{\min}}^{h_{\mathrm{cen}}} \frac{\mathrm{d}h}{h^2} + \frac{1}{\sqrt{2|P-U'(h_{\max})|}} \int_{h_{\min}}^{h_{\max}} \frac{\Pi(h)-P}{h^2\sqrt{h_{\max}-h}}\mathrm{d}h, \tag{A.16}$$

where both integrals at the right-hand side can be integrated analytically. Again expanding the results in $P, \epsilon \to 0$ one obtains

$$I^1_{2,0} \approx \frac{K_9}{\epsilon^2} + O(\epsilon P), \quad K_9 > 1. \tag{A.17}$$

For the integral $I^2_{2,0}$ one obtains:

$$I^2_{2,0} = \int_{h_{\min}}^{h_{\max}} \frac{\sqrt{2R(h)}}{h^3}\mathrm{d}h \le \sqrt{R_{\max}/2}\left(\frac{1}{h^2_{\min}} - \frac{1}{h^2_{\max}}\right) = \frac{1}{6\epsilon^2} + O\left(\frac{P}{\epsilon}\right), \tag{A.18}$$

where $R_{\max} := R(h_c)$ is a maximum of the positive function $R(h)$ which is attained at h_c. Finally from (A.17) and (A.18) one obtains that the integral $I_{2,0}$ is positive for sufficiently small P, ϵ and has the following asymptotics:

$$I_{2,0} \approx \frac{K_{10}}{\epsilon} + O(1), K_{10} > 0. \tag{A.19}$$

One should notice that a similar estimate can be applied to the integral $I_{2,1}$. The only difference here is that the integrand of $I^1_{2,1}$ is improper only at the end $h = h_{\max}$ while is zero at $h = h_{\min}$. Hence the main contribution to $I^1_{2,1}$ comes from $h \to h_{\max}$. The final asymptotics for $I_{2,1}$ is of the form:

$$I_{2,1} \approx K_{11} + O(\epsilon P), \quad K_{11} < 0, \tag{A.20}$$

and hence $I_{2,1}$ is negative.

We summarize that (A.20) together with the fact that the integrals $I_{1,n}$, $n = 0, 1$ defined in (A.2) are positive, because $\bar{h} > h_{\min} > 0$, implies that the denominator of the mobility coefficient is positive for sufficiently small ϵ and P.

References

1. Reiter G (1993) Unstable thin polymer films: rupture and dewetting processes. Langmuir 9:1344–1351
2. Reiter G, Sharma A, Casoli A, David M-O, Khanna R, Auroy P (1999) Thin film instability induced by long range forces. Langmuir 15:2551–2558
3. Seemann R, Herminghaus S, Jacobs K (2001) Dewetting patterns and molecular forces: a reconciliation. Phys Rev Lett 86:5534–5537
4. Redon C, Brochard-Wyart F, Rondelez F (1991) Dynamics of dewetting. Phys Rev Lett 66:715–718
5. Seemann R, Herminghaus S, Jacobs K (2001) Gaining control of pattern formation of dewetting films. J Phys 13:4925–4938
6. de Gennes P (1985) Wetting: statics and dynamics. Rev Mod Phys 57:827
7. Williams MB, Davis SH (1982) Nonlinear theory of film rupture. J Colloid Interface Sci 90:220–228
8. Oron A, Davis SH, Bankoff SG (1997) Long-scale evolution of thin liquid films. Rev Mod Phys 69:931–980
9. Erneux T, Gallez D (1997) Can repulsive forces lead to stable patterns in thin liquid films?. Phys Fluids 9:1194–1196
10. Bertozzi AL, Grün G, Witelski TP (2001) Dewetting films: bifurcations and concentrations. Nonlinearity 14:1569–1592
11. Sharma A, Reiter G (1996) Instability of thin polymer films on coated substrates: rupture, dewetting and drop formation. J Colloid Interface Sci 178:383–389
12. Brochard-Wyart F, Redon C (1992) Dynamics of liquid rim instabilities. Langmuir 8:2324–2329
13. Münch A, Wagner B (2005) Contact-line instability of dewetting thin films. Physica D 209:178–190
14. Limary R, Green PF (2002) Late-stage coarsening of an unstable structured liquid film. Phys Rev E 60:021601
15. Limary R, Green PF (2003) Dynamics of droplets on the surface of a structured fluid film: late-stage coarsening. Langmuir 19:2419–2424
16. Cahn JW, Hilliard JE (1958) Free energy of a nonuniform system. I. Interfacial free energy. J Chem Phys 28:258–267
17. Alikakos ND, Bates PW, Fusco G (1991) Slow motion for the Cahn–Hilliard equation in one space dimension. J Diff Equ 90:81–135
18. Bates PW, Xun JP (1994) Metastable patterns for the Cahn–Hilliard equation: part I. J Diff Equ 111:421–457
19. Bates PW, Xun JP (1995) Metastable patterns for the Cahn–Hilliard equation: part II. Layer dynamics and slow invariant manifold. J Diff Equ 117:165–216
20. Sun X, Ward MJ (2000) Dynamics and coarsening of interfaces for the viscous Cahn–Hilliard equation in one spatial dimension. Stud Appl Math 105:203–234
21. Emmott CL, Bray AJ (1996) Coarsening dynamics of a one-dimensional driven Cahn–Hilliard system. Phys Rev E 54:4568–4575
22. Watson SJ, Otto F, Rubinstein BY, Davis SH (2003) Coarsening dynamics of the convective Cahn–Hilliard equation. J Colloid Interface Sci 22:127–148
23. Glasner KB, Witelski TP (2003) Coarsening dynamics of dewetting films. Phys Rev E 67:016302
24. Glasner KB, Witelski TP (2005) Collision vs. collapse of droplets in coarsening of dewetting thin films. Physica D 209:80–104
25. Neto C, Craig VSJ, Williams DRM (2003) Evidence of shear-dependent boundary slip in Newtonian liquids. Eur Phys J E. doi:10.1140/epjed/e2003
26. Redon C, Brzoska JB, Brochard-Wyart F (1994) Dewetting and slippage of microscopic polymer films. Macromolecules 27:468–471
27. Reiter G, Sharma A (2001) Auto-optimization of dewetting rates by rim instabilities in slipping polymer films. Phys Rev Lett 87:166103
28. Fetzer R, Jacobs K, Münch A, Wagner B, Witelski TP (2005) New slip regimes and the shape of dewetting thin liquid films. Phys Rev Lett 95:127801
29. Münch A, Wagner B, Witelski TP (2006) Lubrication models with small to large slip lengths. J Eng Math 53:359–383
30. Kargupta K, Sharma A, Khanna R (2004) Instability, dynamics and morphology of thin slipping films. Langmuir 20:244–253
31. Brenner MP, Gueyffier D (1999) On the bursting of viscous films. Phys Fluids 11:737–739
32. Glasner K, Otto F, Rump T, Slepjev D (2008) Ostwald ripening of droplets: the role of migration. Eur J Appl Math (Published online by Cambridge University Press, 2 June)
33. Otto F, Rump T, Slepjev D (2006) Coarsening rates for a droplet model: rigorous upper bounds. SIAM J Appl Math 38:503–529
34. Pismen LM, Pomeau Y (2004) Mobility and interactions of weakly nonwetting droplets. Phys Fluids 16:2604–2612
35. Glasner KB (2008) Ostwald ripening in thin film equations. SIAM J Appl Math 69:473–493
36. Gratton MB, Witelski TP (2008) Coarsening of unstable thin films subject to gravity. Phys Rev E 77:016301
37. Peschka D (2008) Self-similar rupture of thin liquid films with slippage. PhD Thesis, Institute of Mathematics, Humboldt University of Berlin
38. Peschka D, Münch A, Niethammer B (2008) Thin film rupture for large slip. J Eng Math (Submitted)
39. Münch A (2005) Dewetting rates of thin liquid films. J Phys 17:309–318